



Article

Tracking Water Quality and Macrophyte Changes in Lake Trasimeno (Italy) from Spaceborne Hyperspectral Imagery

Alice Fabbretto ^{1,2,*}, Mariano Bresciani ¹, Andrea Pellegrino ^{1,3}, Krista Alikas ², Monica Pinardi ¹, Salvatore Mangano ¹, Rosalba Padula ⁴ and Claudia Giardino ^{1,5}

¹ National Research Council, Institute of Electromagnetic Sensing of the Environment, 20133 Milan, Italy; bresciani.m@irea.cnr.it (M.B.); pellegrino.a@irea.cnr.it (A.P.); pinardi.m@irea.cnr.it (M.P.); mangano.s@irea.cnr.it (S.M.); giardino.c@irea.cnr.it (C.G.)

² Tartu Observatory, Department of Remote Sensing, University of Tartu, 61602 Tõravere, Estonia; krista.alikas@ut.ee

³ University of Sapienza, Department of Engineering, 00185 Rome, Italy

⁴ ARPA Umbria, Regional Environmental Protection Agency, 06132 Perugia, Italy; r.padula@arpa.umbria.it

⁵ NBFC, National Biodiversity Future Center, 90133 Palermo, Italy

* Correspondence: fabbretto.a@irea.cnr.it

Abstract: This work aims to show the potential of imaging spectroscopy in assessing water quality and aquatic vegetation in Lake Trasimeno, Italy. Hyperspectral reflectance data from the PRISMA, DESIS and EnMAP missions (2019–2022, summer periods) were compared with in situ measurements from WISPStation and used as inputs for water quality product generation algorithms. The bio-optical model BOMBER was run to simultaneously retrieve water quality parameters (Chlorophyll-a (Chl-a) and Total Suspended Matter, (TSM)) and the coverage of submerged and emergent macrophytes (SM, EM); value-added products, such as Phycocyanin concentration maps, were generated through a machine learning approach. The results showed radiometric agreement between satellite and in situ data, with $R^2 > 0.9$, a Spectral Angle $< 10^\circ$ and water quality mapping errors $< 30\%$. Both SM and EM coverage varied significantly from 2019 (135 ha, 0 ha, respectively) to 2022 (2672 ha, 343 ha), likely influenced by changes in rainfall and lake levels. The areas of greatest variability in Chl-a and TSM were identified in the littoral zones in the western side of the lake, while the highest variation in the fractional cover of SM and density of EM were observed in the south-eastern region; this information could support the water authorities' monitoring activities. To this end, further developments to improve the reference field data for the validation of water quality products are recommended.

Keywords: PRISMA; DESIS; EnMAP; shallow lake; water reflectance; phytoplankton; aquatic vegetation; bio-optical model; machine learning



Citation: Fabbretto, A.; Bresciani, M.; Pellegrino, A.; Alikas, K.; Pinardi, M.; Mangano, S.; Padula, R.; Giardino, C. Tracking Water Quality and Macrophyte Changes in Lake Trasimeno (Italy) from Spaceborne Hyperspectral Imagery. *Remote Sens.* **2024**, *16*, 1704. <https://doi.org/10.3390/rs16101704>

Academic Editors: Andrew Clive Banks, Zhidan Wen, Chong Fang and Shaohua Lei

Received: 27 March 2024

Revised: 2 May 2024

Accepted: 10 May 2024

Published: 11 May 2024



Copyright: © 2024 by the authors. Licensee MDPI, Basel, Switzerland. This article is an open access article distributed under the terms and conditions of the Creative Commons Attribution (CC BY) license (<https://creativecommons.org/licenses/by/4.0/>).

1. Introduction

Lake ecosystems emerge as reliable sentinels of contemporary climate change and anthropogenic processes by providing direct and indirect climate indicators [1,2] and by reflecting alterations in climate patterns and human-induced activities. Monitoring how lakes respond to these influences is crucial because freshwater ecosystems provide a multitude of ecosystem benefits and serve as critical resources for drinking water, agricultural irrigation, biodiversity conservation, industry and recreation [3]. To this end, several regulations have been developed at national and international levels; in particular, the European Commission adopted the Water Framework Directive (WFD, Directive 2000/60/EC), which establishes a unified framework for integrated water resource management in the European Union (EU) [4,5]. Its central purpose is to establish a comprehensive framework dedicated to safeguarding and promoting the sustainable management of water resources throughout the EU member states, with the aim of collectively achieving a “good ecological status” for all water bodies. The WFD is applicable to inland, transitional and coastal surface

waters, as well as groundwater, and indicates the parameters to be monitored and the frequency of monitoring, thus helping inform adaptive strategies for managing these vital natural resources [6]. Among those indicated for monitoring, the key parameters are those related to the ecological status of water bodies, in particular Chlorophyll-a (Chl-a), which is considered a proxy for phytoplankton biomass and therefore contributes to defining the trophic status of a water body [7]; Total Suspended Matter (TSM), which is a tracer for inflowing pollutants and is related to water transparency [8,9] and Phycocyanin (PC), which is a photosynthetic auxiliary pigment that is abundant in cyanobacteria [10–12].

Macrophytes are important elements of inland waters [13,14], increasing their ecosystem services (e.g., carbon sequestration, habitat provision, nutrient uptake) and fulfilling a central role in the cycling of elements in aquatic ecosystems [15,16]. The complex interactions between physical, chemical and biological processes in surface waters lead to significant challenges for in situ monitoring and often limit the ability to adequately capture the dynamics of aquatic systems and to understand their status, functioning and response to pressures. In this context, the use of remote sensing allows for wide spatial coverage and regular monitoring frequency, providing information on water conditions, bottom properties and the presence and abundance of aquatic plants, distinguishing them into different association types; this complements traditional in situ measurements [17–22]. The reviews reported in [23,24] highlighted the significant increase in remote sensing studies of inland water quality, due both to improved access to Earth Observation (EO) data and increasing computational capabilities. Particularly, imaging spectroscopy has gained wide interest [25–28], as the collection of data in narrower, contiguous bands is improving aquatic ecosystem mapping for the simultaneous retrieval of parameters describing water quality and aquatic vegetation (e.g., biomass [29] and the identification of invasive species [30]). In the last few years, hyperspectral spaceborne and airborne images have been providing significant advances in algorithm development and innovative mapping tools [31,32]. For instance, the PRecursoRE IperSpettrale della Missione Applicativa (PRISMA) and the DLR Earth Sensing Imaging Spectrometer (DESI) products were exploited for the estimation of optically active parameters (Chl-a, TSM) in Italian lakes with different optical properties [33], and for one of these lakes (i.e., Trasimeno), PRISMA water quality products were evaluated with respect to Sentinel-2 in [34]. DESI data were also used for mapping water quality parameters in lagoons and estuaries [35]. Furthermore, PRISMA spectral features enabled distinctions to be made between shallow and turbid waters [36], while in [37], PRISMA products were used to develop novel algorithms for the estimation of cyanobacteria biomass in lake Trasimeno. PRISMA products were also exploited for the detection of floating plastic materials through unsupervised and supervised machine learning approaches [38].

In the wake of these works, this study presents a relevant multitemporal dataset compiled using three flying spaceborne imaging spectroscopy missions for enabling aquatic ecosystem mapping. A set of sensor-independent algorithms for deriving water quality parameters in optically complex waters is applied to all imagery data. In particular, the study builds on 13 hyperspectral reflectance products of Lake Trasimeno (Italy) provided by PRISMA, DESI and the Environmental Mapping and Analysis Program (EnMAP). The dataset covers the summer periods from 2019 to 2022 (from early June to mid-October) to assess changes in water quality parameters and aquatic vegetation coverage and type, upon having verified the accuracy of satellite-derived products with corresponding in situ measurements [39–45] in terms of remote sensing reflectance (Rrs), a key parameter that is widely used for aquatic applications [46]. Reference in situ measurements are provided by the WISPStation, an autonomous fixed-position radiometer that provides continuous Rrs measurements, from which an estimate of bio-geophysical parameters can also be derived [47]. The Rrs products derived from spaceborne hyperspectral observations are then exploited as inputs for the simultaneous mapping of water quality (Chl-a, TSM, PC) and aquatic vegetation. Several environmental parameters, such as water level fluctuations, are considered to discuss the spatio-temporal changes.

2. Data and Methods

2.1. Study Area

Lake Trasimeno, which is located in central Italy (43.138N, 12.113E), is the only Italian lake of tectonic origin and fourth in size, with an area of 124 km². The lake is nearly round in shape with a diameter of about 12 km, with three small islands. It is a closed lake, with un-stratified and very shallow waters (average bottom depth, 4.7 m; maximum depth, 6 m) characterized by banks with minimal slopes and, in the south-eastern area, an open bay colonized by aquatic vegetation: permanently submerged (e.g., *Chara globularis*) and semi-emergent macrophytes (in some seasonal phases of their life cycle, they can emerge from the water–atmosphere interface with flowers, fruits and part of the plant body, e.g., *Potamogeton pectinatus*, *P. perfoliatus*, *Myriophyllum spicatum* and *Ceratophyllum demersum*) [48]. These are among the most common species present in Italian lakes; they are also found in the large subalpine lakes of Northern Italy [49,50]. The lake is part of Tevere River Basin, which is connected to the hydrographical network of the Nestore River by an artificial outfall built with the function of flood regulation. The gradual lowering of the lake's level, though, has made this connection non-functional for almost a decade; the waters have not reached the overflow level since 2015 [51]. Stopping—or at least drastically decreasing—water withdrawals may not be the ultimate solution to the basin's hydrological problems. Nevertheless, it would be a substantial benefit for a lake that depends on water resources that are crucial to maintaining the balance of its delicate environmental state, and to sustain several vital economic activities, such as agriculture, fishing and tourism. The lacustrine ecosystem is an area of exceptional value due to its wealth of flora and fauna and its diversity of species, and in 1995, it was declared a protected area (regional law L.R. 9, 03/03/1995). Tourism, agriculture and livestock farming are the most present activities in the Lake Trasimeno area; approximately 70% of the lake's catchment area is enveloped by cultivated land, while intensive agriculture requiring irrigation occupies 28% of this territory. As a result, these activities have contributed to the eutrophication phenomenon in the lake [52]. The lake ranges from mesotrophic to eutrophic conditions [43], where the principal critical parameters for the ecosystem status are phosphorous and nitrogen. In the past few years, the lake has hence encountered challenges in recovering equilibrium as recommended by the WFD. This situation is aggravated by the lack of natural outlets and a limited water inflow (Paganico and Pescia streams); for its water supply, the lake relies exclusively on small streams and precipitation. The water level began to decline in the 1990s, and at the end of 2022, it was 1.3 m below the hydrometric zero [53]. Therefore, the hydrographic characteristics of the lake (width, shallowness, low water exchange, etc.) determine a strong influence of temperature and light conditions, which favor an increase in Chl-a, especially starting from spring and reaching its peak at the end of summer. This phenomenon is indeed closely linked to the presence of and increase in aquatic plants and algal blooms.

2.2. Data Collection

2.2.1. In Situ Data

Reference data were obtained from the Remote Sensing for Trasimeno lake Observatory (RESTO) field infrastructure, where high-frequency in situ measurements are collected by means of a WISPStation mounted on a platform located 100 m north of Polvese island (Figure 1) [19,20].

From April 2018, the WISPStation has been collecting, every 15 min, Rrs data (in the spectral range of 350–900 nm with a spectral resolution of 4.6 nm) along with Chl-a, TSM and PC concentrations, as derived from the measured Rrs through standard water quality algorithms [54–58]. For both Rrs and water quality data, a set of three measurements closest to the acquisition time of the satellite overpasses were selected to calculate the mean and standard deviation. The Rrs data collected by the WISPStation were spectrally resampled to the band settings of PRISMA, DESIS and EnMAP to perform a radiometric comparison.

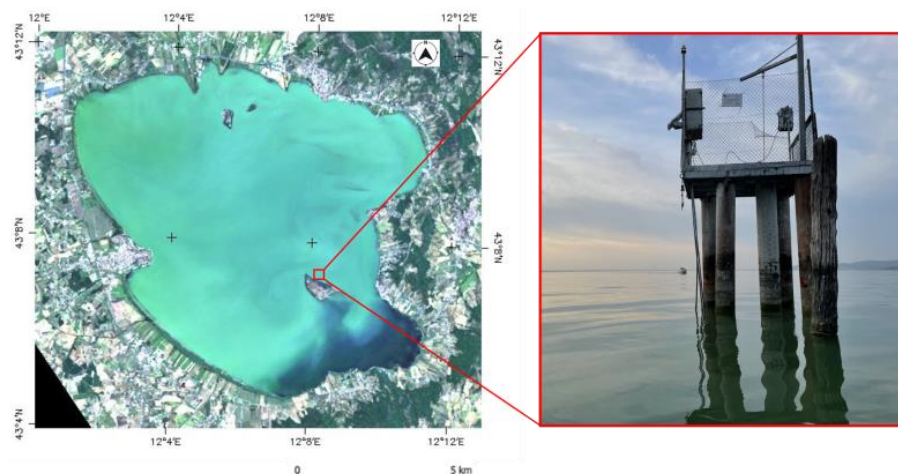


Figure 1. On the left, a true color composition image as acquired by DESIS on 4 August 2019 showing the position of the WISPStation (43.122, 12.134—red box); on the right, a picture of the platform with the WISPStation.

With ± 5 days close to the dates of the images' acquisitions, ad hoc in situ campaigns were also organized to survey the optically deep and optically shallow areas, and for the latter to detect the different cover classes, with the visual GPS positioning method, as used in [59]. GPS ground truths were then used for an accuracy assessment of the satellite-derived maps.

The hydrographic service of the Umbria region [53] provided air temperature, precipitation data and lake water levels for the investigated temporal range from January 2019 to December 2022, as shown in Figure 2. The inventory of the sampling of birds feeding on macrophytes (e.g., *Anas* sp., *Aythya* sp. and *Fulica* sp.) provided by “Regione Umbria—Osservatorio Faunistico Regionale” [60] showed the following number of birds for the study period: 43'397 (in 2019), 29'377 (in 2020), 43'382 (in 2021) and 40'707 (in 2022).

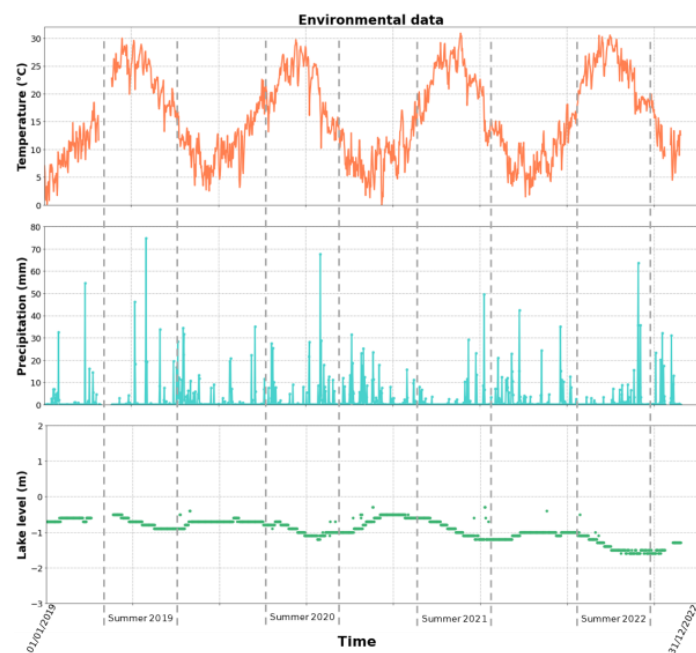


Figure 2. Time series of the environmental data: air temperature ($^{\circ}\text{C}$) shown in orange, precipitation (mm) shown in light blue and lake level (m) shown in green. The four summer periods in which satellite images were acquired are highlighted in grey with dashed lines.

2.2.2. Spaceborne Data

The imagery data used in this study were gathered from three hyperspectral spaceborne missions: PRISMA, DESIS and EnMAP. The data can be downloaded from the respective catalogues, at different levels of processing: Level 1 (L1) are images in terms of the radiance measured at the sensor (Top of Atmosphere, TOA) and Level 2 (L2) represents the atmospherically corrected ground reflectance (Bottom of Atmosphere, BOA) data. Following a short overview of the three sensors and their main applications, the key characteristics of each are shown in Table 1.

PRISMA, operated by the Italian Space Agency (ASI), is a single satellite placed in low-Earth Sun-synchronous orbit (SSO-LTDN), with a revisit time of 29 days, a period that can be reduced to 7 days thanks to platform roll maneuvers [61]. The payload includes a medium-resolution hyperspectral camera (HYP) and a high-resolution panchromatic camera (PAN), which may support finer-scale mapping [62]. The PRISMA mission was designed to advance technology qualifications, develop applications and provide environmental observation and risk management products to both institutional and scientific users [63]. PRISMA L2 products (version 02.05) are those obtained from TOA radiance products (L1) after automatic land-based atmospheric correction based on MODTRAN v 6.0 [43,44].

DESI is a hyperspectral instrument integrated into the Multi-User-System for Earth Sensing (MUSES) platform installed on the International Space Station (ISS). The mission is operated by the German Aerospace Center (DLR). The spectral and spatial resolution of the sensor allow new developments for a wide range of applications in very different environments, such as inland and coastal waters, the cryosphere and vegetation [64,65]. DESIS L2 products (version 2.20) are those obtained from TOA radiance products (L1) after automatic land-based atmospheric correction performed with Python-based Atmospheric Correction (PACO) [66].

EnMAP is a high-resolution imaging spectroscopy remote sensing mission, operated by the DLR, placed in SSO-LTDN. The across-track tilt-capability of 30° enables revisit times of less than four days [67]. The primary objective of the mission is to assess and examine surface variables, both qualitative and quantitative, that characterize essential Earth processes [68]. These variables are obtained on a global scale in a routine and consistent way. EnMAP L2 products (version v01.04.00) can be obtained through two individual sub-processors for the atmospheric correction of orthorectified TOA radiance both over land (PACO) and water surfaces (Modular Inversion Program, MIP [69]) [70].

Table 1. List of the main features of the PRISMA, DESIS and EnMAP payloads [71–73].

	PRISMA	DESI	EnMAP
Launch	22 March 2019	29 June 2018	1 April 2022
Coverage	70°N to 70°S	55°N to 52°S	Global in near-nadir mode
Ground sampling distance	HYP: 30 m; PAN: 5 m	30 m	30 m
Number of bands	HYP: 240 [400–2500 nm] PAN: 1 [400–700 nm]	235 (no binning) 60 (binning) [400–1000 nm]	246 [420–2450 nm]
Radiometric resolution	12 bits	13 bits + 1 bit gain	≥14 bits
Atmospheric correction	MODTRAN v 6.0 (land based)	PACO (land)	PACO (land) MIP (water)

Overall, a total of 13 hyperspectral data with cloud coverage of less than 10% (apart from PRISMA acquired on 3 June 2020) were available for Lake Trasimeno, as presented in Table 2.

Table 2. Spaceborne data of Lake Trasimeno: sensor, date and UTC acquisition time.

Sensor	Date	UTC Time
PRISMA	4 June 2019	10:15
PRISMA	26 July 2019	10:13
DESIS	4 August 2019	13:33
DESIS	5 September 2019	06:49
PRISMA	3 June 2020	10:10
PRISMA	25 July 2020	10:07
DESIS	4 June 2021	12:20
DESIS	15 October 2021	13:47
DESIS	19 June 2022	16:10
PRISMA	20 July 2022	10:08
DESIS	7 August 2022	10:50
PRISMA	12 August 2022	10:04
EnMAP	5 October 2022	10:40

2.3. Methodology Process Flowchart

This section reports a flowchart (Figure 3) of the methodology used in this study, from the hyperspectral reflectance data gathered by PRISMA, DESIS and EnMAP to the spatio-temporal analysis of the changes in Lake Trasimeno that occurred in terms of water quality parameters and bottom coverage.

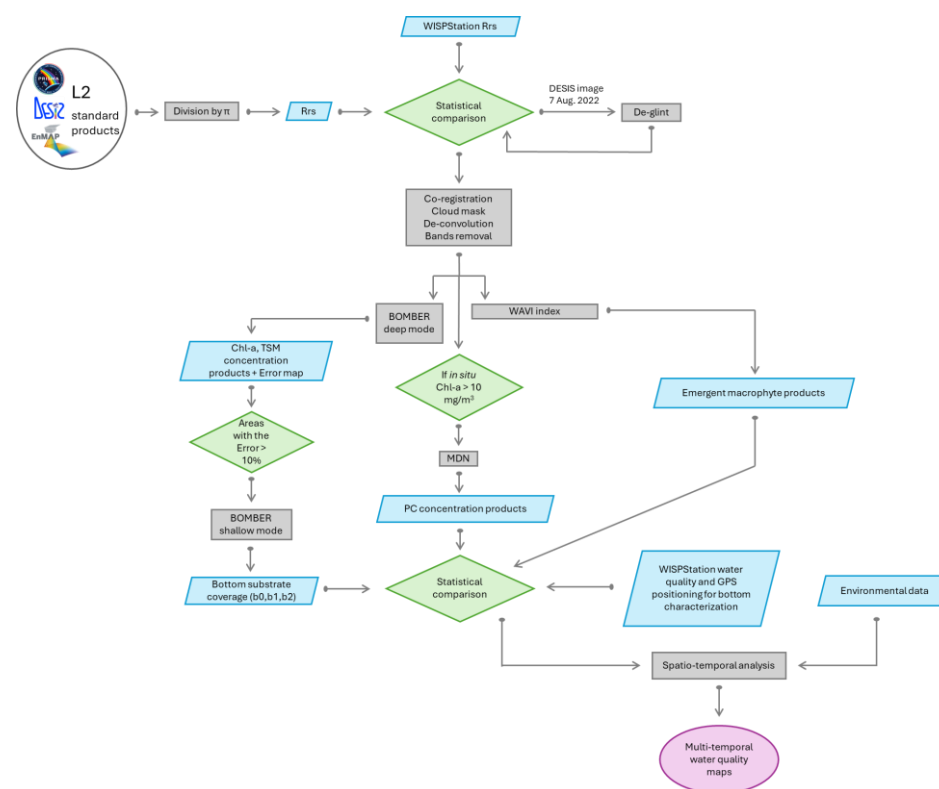


Figure 3. Flowchart of the methodology applied in the study. The oval with a black outline represents the input products where the study started from. Grey boxes indicate the methodology applied. Green diamond shapes stand for decision-making steps in the process. Blue parallelograms represent products generated, and the violet oval indicates the end point of the process.

In the following Sections (Sections 2.4–2.7) a detailed description of the methodology is presented.

2.4. Image Pre-Processing

The PRISMA, DESIS and EnMAP (MIP-based atmospheric correction) L2 products were downloaded in the visible–near-infrared (VNIR, i.e., 400–1000 nm) region of the spectrum from the respective space agencies' portals, and a division operation by π was performed to obtain the most used quantity in aquatic applications, which is Rrs. One image (DEGIS, 7 August 2022) was affected by sun glint, which represents a disturbance and alteration of the Rrs. Hence, a sun glint correction method based on a negligible signal in the near-infrared (NIR) part of the spectrum was performed, using the algorithm proposed in [74]. Particularly, the relative intensity of the solar glint in the image was obtained from the NIR brightness and the light in the visible (VIS) band using a set of pixels that could be homogeneous were it not for the presence of the glint. By establishing a linear relationship between the NIR bands and each VIS band, the contribution of the sun glint could be removed. The removal was performed by applying the de-glint processor implemented in the SNAP software (version 9.0.0) "Sen2Coral toolbox", providing the DESIS L2 Rrs product as an input.

Before the Rrs data could be used as inputs in the product generation algorithms, several operations were carried out to improve the products themselves, aiming to obtain final maps that are more accurate and representative of the real state of the target [75,76]. First, co-registration of the images was carried out both to adjust the georeferencing and to identify the lake area by using the shapefile of the lake delivered by OpenStreetMap. The cloudy pixels were masked using the threshold proposed by [77]. Given the low signal of the water bodies, the machine learning algorithm could add a salt-and-pepper noise effect to the results; hence, a deconvolution—with a 5-pixel median window filter—was applied to increase the signal [78]. As recommended by [44] concerning PRISMA data specifically, the preserved spectral range (450–800 nm) was standardized for all the sensors, resulting in having 40 bands for PRISMA, 34 for DESIS and 61 for EnMAP images. The last step before product generation was to identify the portion of the lake covered by emergent macrophytes. To this end, the WAVI index [79] was calculated to detect the coverage of emergent macrophytes (positive values of WAVI) and to assess indications of their morphological traits (as a proxy of biomass index).

2.5. Algorithms for Aquatic Ecosystem Mapping

2.5.1. BOMBER

The spectral inversion procedure was performed with the BOMBER ('Bio-Optical Model-Based tool for Estimating water quality and bottom properties from Remote sensing images') code, which implements the algorithms presented in [80,81] for deriving water column and bottom properties via a non-linear optimization technique. The software employs bio-optical models for both optically deep and shallow waters; the model determines mathematical equations between the Rrs and the inherent optical properties of the optically active constituents, as well as the concentrations of water quality parameters and bottom properties (e.g., fractional cover up to three bottom types). As inputs to the code, the imagery data atmospherically corrected to Rrs, the mask of the area of interest, the definition of the model type (deep or shallow mode) and the setting of the model parameters (absorptions and backscattering coefficients, starting values, etc.) were provided. In this work, BOMBER, parameterized with the intrinsic optical properties specific for Lake Trasimeno [33], was run for all the images in deep water mode to generate Chl-a and TSM concentrations. The model was initialized with the average values of water quality parameters resulting from coincident measurements of Chl-a and TSM inferred from Rrs data gathered at the time of sensor overpasses from the WISPStation. The absorption of Colored Dissolved Organic Matter (CDOM) at 440 nm was not retrieved due to the lack of in situ data for its parametrization, but it was set constant to the average concentration of the lake and equal to 0.25 m^{-1} . The specific absorption spectra of phytoplankton for Lake Trasimeno were selected depending on the month/period, due to the change in phytoplankton concentration and composition (June: clear water without cyanobacteria,

July–October: higher phytoplankton biomass and higher presence of surface cyanobacteria). Other parameters whose change might have an impact on the retrieval of water quality parameters, such as the conversion factor of the absorption of Non-Algal Particles at 440 nm to TSM, were adjusted based on the optical closure between the modeled Rrs and measured Rrs over the deep water station of the WISPSStation. In the areas where the optical closure error was greater than 10% [31], the model was then run in shallow water mode. The three bottom coverage classes—named in BOMBER as “b0”, “b1” and “b2”—were thus assigned: b0 = high-albedo vegetation (semi-emergent macrophytes); b1 = low-albedo vegetation (permanently submerged macrophytes); b2 = un-colonized pixels (sand).

2.5.2. Mixture Density Network

The Mixture Density Network (MDN) algorithm was calibrated in [37] considering resampled in situ radiometric measurements for the Hyperspectral Imager for the Coastal Ocean (HICO) and PRISMA sensors. The dataset of the mentioned work consisted of a large number of samples of in situ measurements of Rrs, Chl-a and PC for water bodies worldwide (including Lake Trasimeno). The MDN uses band ratios, line heights and operational algorithms based on the correlation between Rrs and PC. Since the algorithm does not allow any setting of additional parameters, the MDN was applied in the default mode [82]. As inputs to the model, PRISMA images were provided considering the specific subset of bands from 504 to 723 nm. To exploit the entire dataset, DESIS and EnMAP images were resampled according to the spectral configuration of PRISMA between 504 and 723 nm, for which the retrieving PC algorithm was validated. PC concentration maps were generated for the imagery data showing a Chl-a concentration greater than 10 mg/m³, as recommended by [83].

2.6. Product Validation

Common statistical metrics were used to assess the agreement of Rrs and water quality products between satellite and in situ data. In the following equations, n represents the number of concurrent observations, and x_i and y_i are the sensors-estimated Rrs data and in situ measurements, respectively. For the comparison, Regions of Interest (ROIs) with a size of 5 × 5 pixels were extracted from the satellite images and water quality maps and the mean and standard deviation were calculated.

The coefficient of determination (R^2), that is, the proportion of the variance in the dependent variable that is predictable from the independent variable, was computed as follows:

$$R^2(/) = \frac{[\sum (x_i - \bar{x})(y_i - \bar{y})]^2}{\sum (x_i - \bar{x})^2 \sum (y_i - \bar{y})^2}$$

The Root Mean Square Difference (RMSD), that is, a measure of the differences between values predicted by an estimator and the values observed, was calculated as follows:

$$RMSD (sr^{-1}) = \sqrt{\frac{\sum (x_i - \hat{y}_i)^2}{n}}$$

The Spectral Angle (SA), that is, a measure for directly comparing image spectra to in situ spectra, and determining how similar the spectra shapes are, was derived as follows:

$$SA (^\circ) = \cos^{-1} \frac{\sum y_i x_i}{\sqrt{\sum y_i^2} \sqrt{\sum x_i^2}}$$

The Mean Absolute Percentage Difference (MAPD), that is, a measure used to quantify the average percentage difference between two samples, was obtained as follows:

$$MAPD (\%) = \frac{100}{n} \sum \left| \frac{x_i - y_i}{y_i} \right|$$

Control points were used to compare in situ data and satellite-derived maps. The product accuracy was quantified using a confusion matrix, selecting four different classes.

2.7. Spatio-Temporal Analysis

Following the validation of the products, a spatio-temporal analysis was carried out to quantify the changes in primary producers' community abundance and coverage in the different summer periods investigated. To quantify the presence of aquatic vegetation, the areas of submerged macrophytes (obtained by summing the two cover classes provided by BOMBER, "b0" and "b1") and emergent macrophytes were first calculated. Additionally, a more detailed analysis of the three bottom coverage classes was carried out by calculating the fractional cover by labeling a pixel as "sand" where $b2 > 0.66$ (66%) and distinguishing three different classes of submerged macrophytes as follows: sparse ($0 < b0 + b1 < 0.4$), moderate ($0.4 < b0 + b1 < 0.7$) and dense ($b0 + b1 > 0.7$). This was carried out following similar work [50] conducted over Lake Garda, where the same macrophyte species are present as on Lake Trasimeno, and in both cases, the method for classifying the colonized substrate as "sparse", "moderate" and "dense" is generic and does not depend on the characteristics of the site, so similar thresholds can be used. Finally, to assess the variability in the water quality parameters and of the aquatic vegetation, the products obtained were integrated to perform a spatio-temporal analysis with the GRASS GIS algorithm "r.series", which allowed us to make each output pixel value a function (i.e., mean and standard deviation) of the values associated with the corresponding pixels in the input list of maps.

3. Results

3.1. Radiometric Validation

The removal of the sun glint from the image affected by this disturbance (DESIS 7 August 2022) led to the result shown in Figure 4.

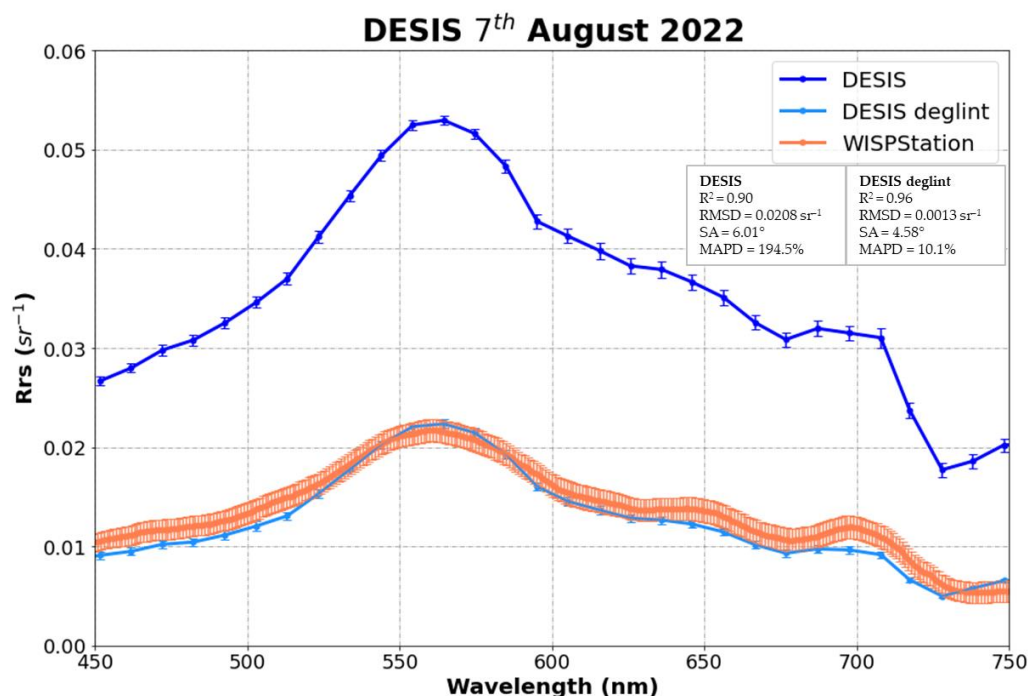


Figure 4. Comparison of DESIS and in situ Rrs data, before ("DESIS", dark blue) and after ("DESIS deglint", light blue) sun glint removal. In situ data are displayed in orange. Statistical results are displayed in the boxes.

As can be seen, the level of agreement between the satellite data and in situ measurement increased after the sun glint correction. There is an improvement in the fitting between the Rrs spectra in terms of magnitude (MAPD reduced by 95%), while the SA value, referring to the spectral similarity, remains almost constant.

Figure 5 shows the radiometric validation of all the satellite-derived Rrs products, based on the comparison with in situ data.

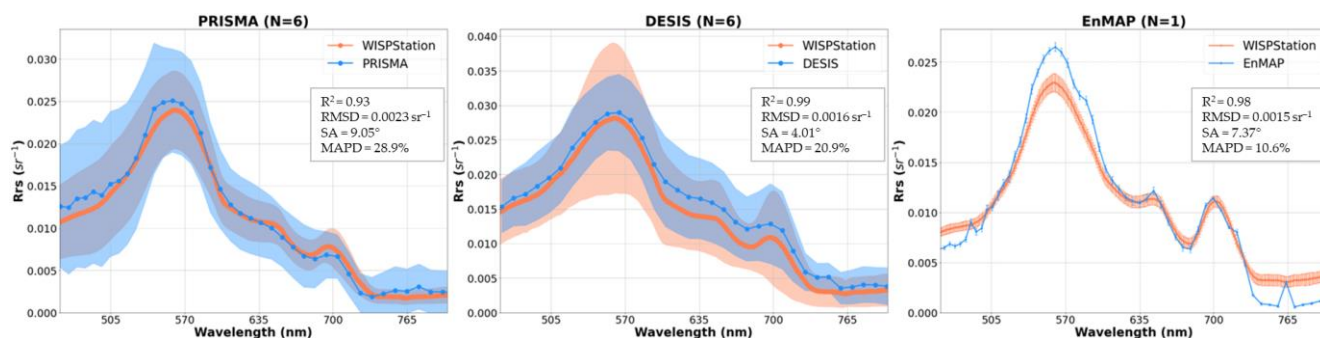


Figure 5. Comparisons of the average Rrs values gathered from the spaceborne data and corresponding in situ Rrs data. The variability in the mean spectra of PRISMA (6 images) and DESIS (6 images) is displayed as blue curves, with the shaded blue area representing the standard deviation. The mean and standard deviation of the in situ data are equivalently shown in orange. In the case of the EnMAP data, the comparison is limited to a single image, and it is shown with the same color configuration. In this case, the standard deviation refers to the variability present in the ROI and in the set of three measurements of the in situ data. The statistical results are displayed in the boxes.

Overall, the Rrs data derived from the three missions show agreement with the in situ measurements, over the entire spectrum between 450 and 800 nm, with values of SA below 10° and values of MAPD below 30%. The satellite-derived Rrs data consistently show spectral features due to the presence of PC (620, 650 nm) and Chl-a (680, 700 nm).

3.2. Water Quality Product Generation and Validation

Proceeding forward, the generated water quality maps (Chl-a, TSM, PC) are shown along with their validation (Table 3, Figure 6). The last row of the table (*) shows the validation considering samples containing all the data from the different sensors.

Table 3. Statistical validation of Chl-a, TSM and PC concentration maps, in terms of RMSD and MAPD. N is the number of the images in the sample.

Product	N	Chl-a		N	TSM		N	PC	
		RMSD (mg/m ³)	MAPD		RMSD (g/m ³)	MAPD		RMSD (mg/m ³)	MAPD
PRISMA	6	3.30	29.8%	6	3.10	19.9%	4	3.85	27.3%
DESIS	6	3.92	25.2%	6	1.85	9.6%	4	2.70	22.4%
EnMAP	1	1.42	6.5%	1	3.38	20.2%	1	2.50	25.5%
*	13	3.32	23.8%	13	2.71	15.6%	9	3.31	25.3%

Considering PRISMA and DESIS, which present a greater number of images in the dataset, for the Chl-a and TSM products generated by the BOMBER bio-optical model, the highest level of agreement is obtained in the case of the maps generated from DESIS images for the estimation of TSM (MAPD = 9.6%). Regarding the estimation of Chl-a, the level of agreement is lower, with a MAPD of over 20% both in the case of PRISMA and DESIS products. The statistical analysis of EnMAP is slightly weaker (N = 1), but it achieved RMSD and MAPD values comparable with those of PRISMA and DESIS and the highest level of agreement in the case of Chl-a estimation. In the case of the PC products generated

through the MDN, the level of agreement obtained by the three sensors is similar, with slightly higher accordance in the case of the product given by EnMAP. Overall, MAPD values $\leq 30\%$ are obtained in all cases.

The validation through visual GPS positioning led to an Overall Accuracy of 89.1% for the four classes considered, as shown in Table 4.

Table 4. Confusion matrix for the validation of the four classes selected: b2 (sand), b0 + b1 (submerged aquatic vegetation), EM (emergent macrophytes), deep water.

		Spaceborne Images				Total
		b2	b0 + b1	EM	Deep Water	
In situ	b2	7	2			9
	b0 + b1	2	13			15
	EM			6		6
	Deep Water		1		15	16
	Total	9	16	6	15	
Overall Accuracy					89.1%	

Next, Figure 6 illustrates the entire dataset of the water quality products in terms of Chl-a, TSM and PC in the portion of the lake that presented optically deep waters and, in the last column, the mapping of the emergent macrophytes and the three types of bottom cover classes (sand, permanently submerged and semi-emergent macrophytes) in the portion that presented optically shallow waters. The areas of the images affected by clouds are indicated by a grey color.

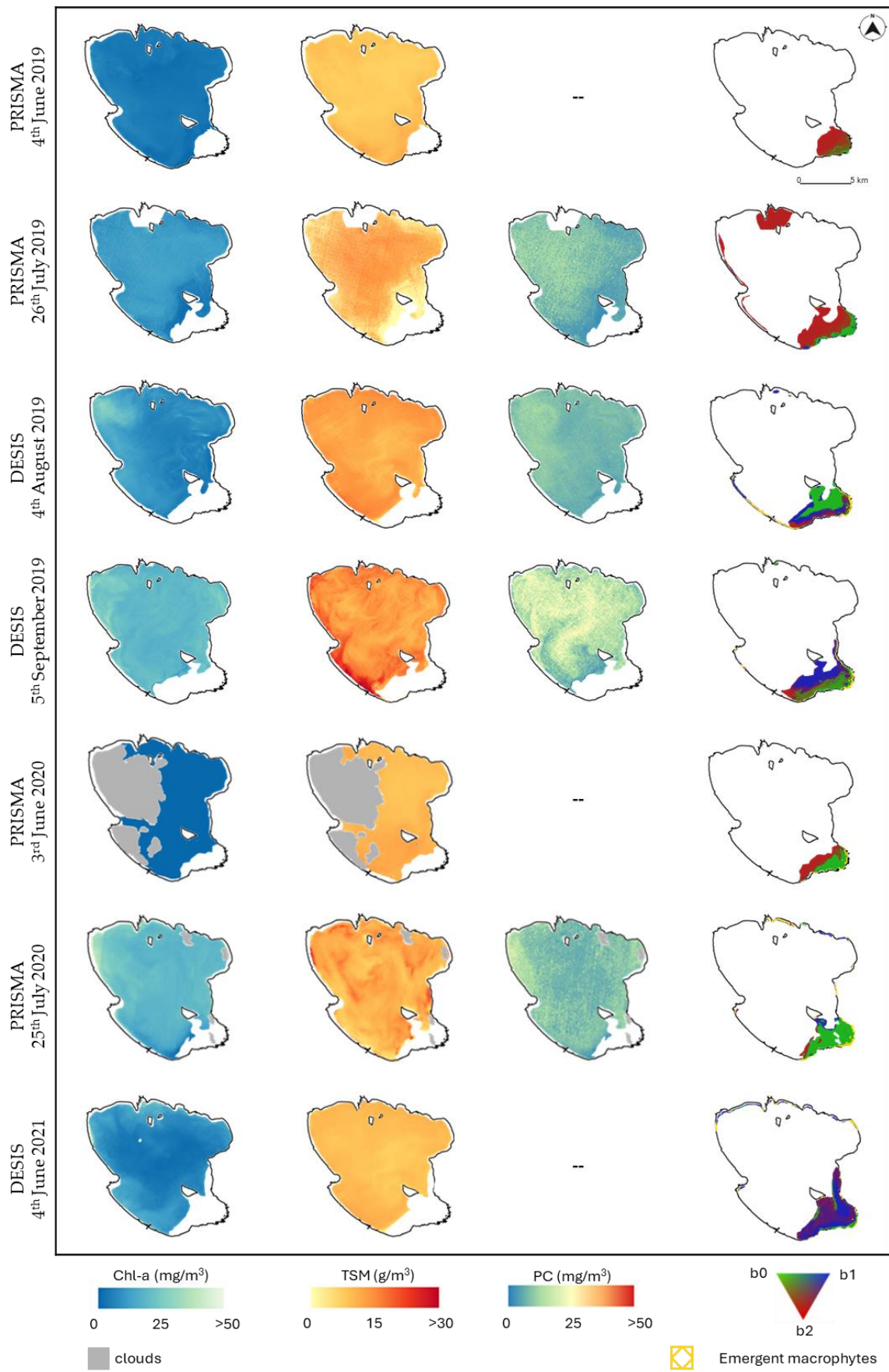


Figure 6. Cont.

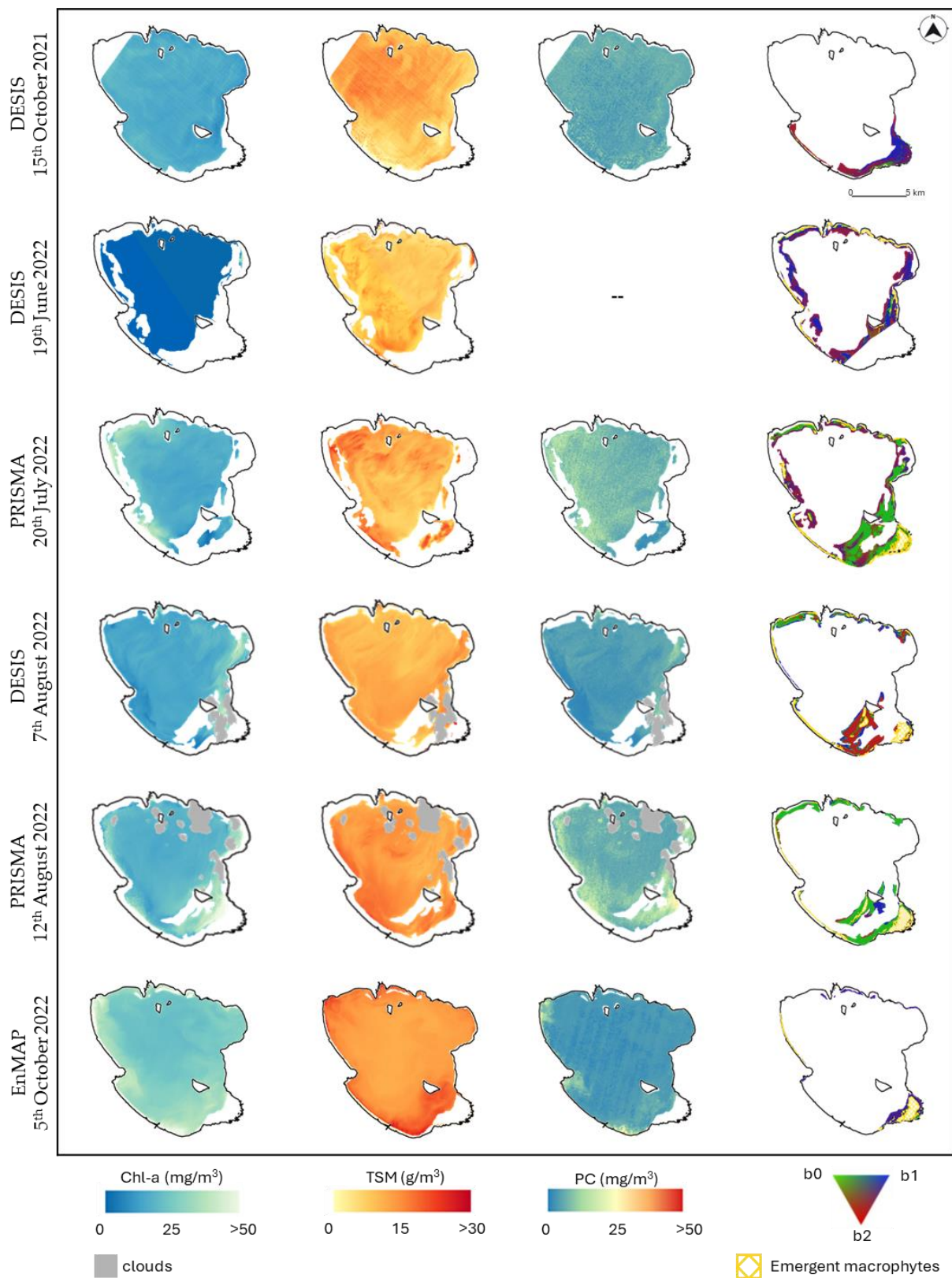


Figure 6. Water quality maps and bottom characterization for the 13 images of the available dataset. From left to right: Chl-a, TSM and PC maps; bottom characterization products, in terms of emergent macrophytes and the three cover classes: b0 (semi-emergent macrophytes), b1 (permanently submerged macrophytes), b2 (sand).

The maps show the temporal and spatial variation in the water quality parameters in the lake from June 2019 to October 2022 (summer periods). As is evident from the maps, the lowest values of Chl-a (up to 1 mg/m³) and TSM (up to 1 g/m³) are detected in June. Higher values, instead, occur in the following summer months for both parameters; the maximum values are generally observed in September–October. PC maps were generated for images from which a Chl-a value higher than 10 mg/m³ was derived. Indeed, there are no PC maps for the months of June; the highest PC values are achieved in September. Regarding the optically shallow water areas, the area of submerged and emergent macrophytes increases over the years, not only in the south-easternmost part of the lake, but also along the littoral zone of the northernmost part of the lake.

3.3. Spatio-Temporal Analysis

The area of the submerged (sum of “b0” and “b1”, whatever the coverage degree) and emergent macrophytes (positive WAVI) retrieved for the period investigated is shown in Table 5. The percentages were calculated with respect to the water cloud-free pixels’ area.

Table 5. Area in hectares of submerged and emergent macrophytes across various dates in the dataset. In brackets, the percentages that the values represent over the total number of water pixels not covered by clouds.

Product	Submerged Macrophytes	Emergent Macrophytes
PRISMA 4 June 2019	135 ha (1.1%)	0 ha
PRISMA 26 July 2019	287 ha (2.4%)	0 ha
DESIS 4 August 2019	1140 ha (10.1%)	52 ha (0.5%)
DESIS 5 September 2019	1190 ha (10.3%)	25 ha (0.2%)
PRISMA 3 June 2020	300 ha (3.4%)	19 ha (0.2%)
PRISMA 25 July 2020	878 ha (7.9%)	37 ha (0.3%)
DESIS 4 June 2021	1523 ha (13.6%)	33 ha (0.3%)
DESIS 15 October 2021	601 ha (5.1%)	3 ha (<0.1%)
DESIS 19 June 2022	1790 ha (16.7%)	149 ha (1.4%)
PRISMA 20 July 2022	2672 ha (23.0%)	336 ha (2.9%)
DESIS 7 August 2022	1350 ha (12.3%)	324 ha (3.0%)
PRISMA 12 August 2022	1223 ha (11.7%)	343 ha (3.3%)
EnMAP 5 October 2022	344 ha (3.0%)	199 ha (1.7%)

These values reveal that, in addition to the seasonal vegetative cycle with growth starting in early summer and a senescence period in late summer for both submerged and emergent macrophytes, there is an unprecedented increase—in terms of area—in July 2022, leading to an increase of approximately 160% in submerged macrophytes and 600% in emergent macrophytes compared to the average values for the period 2019–2021. The values of the WAVI index show that in 2022, at the maximum area of emergent macrophytes (343 ha, 12 August 2022), the maximum WAVI value was recorded to be 0.38, which corresponds to an increase of about 240% compared to the date with the lowest WAVI value (0.11, on 15 October 2021).

The fractional coverage analysis during the study period is shown in Figure 7.

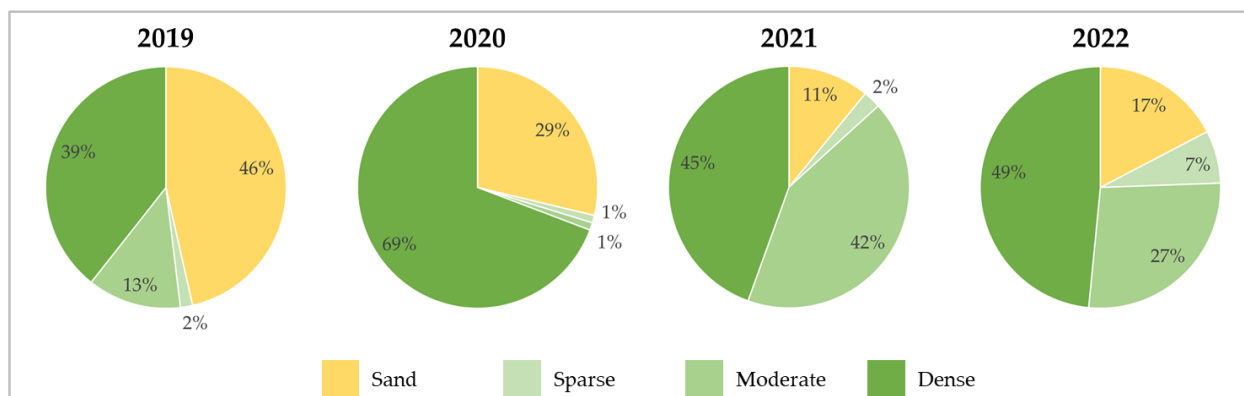


Figure 7. Distributions of sand and submerged macrophyte cover classes (sparse, moderate and dense) in the four-year study period. Un-colonized (sand) pixel percentage is represented in yellow; sparse, moderate and dense submerged macrophytes are shown with a gradient of green from lightest to darkest.

These results show how the fractional cover of the different classes changed over the study period. Un-colonized pixels representing a substrate covered by sand, for instance, decreased considerably in 2021 and 2022, compared to the initial value in 2019. At the same time, the substrate covered by submerged macrophytes increased (moderate and dense classes).

The results of the spatio-temporal analysis showing the areas of highest variability in water quality parameters (Chl-a, PC, TSM), submerged macrophytes' fractional cover and emergent macrophytes' density are presented in Figure 8.

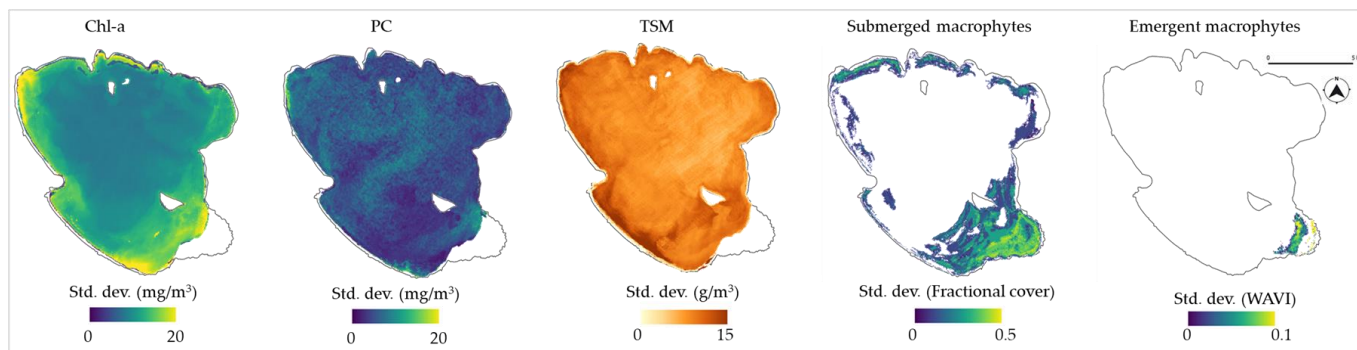


Figure 8. From left to right, standard deviation maps of Chl-a, PC, TSM, submerged macrophytes' fractional cover and emergent macrophytes' density (WAVI).

The Chl-a values show greater variability (up to 20 mg/m^3) in the portions of the lake closer to the littoral zone. The PC concentrations show higher variability in the littoral part of the lake (up to 17 mg/m^3) than for Chl-a, and in the open water part of the lake (up to 10 mg/m^3). The TSM concentrations show higher variability close to the tributary inflow in the south-western part of the lake, with values around 15 g/m^3 . Macrophytes show higher variability in terms of fractional cover (up to 50%) and density in the south-eastern part of the lake where the aquatic vegetation is well established.

4. Discussion

Rrs is the core product of the optical remote sensing of water bodies and is used to retrieve water quality parameters. Given the importance of its function, it is therefore crucial to assess its accuracy [84–88]. In the present study, Rrs data from hyperspectral sensors PRISMA, DESIS and EnMAP over Lake Trasimeno were validated through comparison with in situ data, provided by the WISPStation. A total of 13 standard L2 products provided

by the respective space agencies were pre-processed to ensure geographic co-registration, to mask clouds, to remove sun glint when present and to decrease the environmental noise over water. Notably, only one of the 13 images was affected by sun glint, most likely due to favorable observation/illumination geometries. Although the process of sun glint removal resulted in the loss of bands in the NIR region for the DESIS data acquired on 7 August 2022, there is a significant improvement in agreement with the in situ measurement. The MAPD value is significantly reduced, while the SA value, related to spectral similarity, remains almost constant; this result is consistent with assumption that the sun glint disturbance leads to an alteration mainly in the magnitude of the signature, rather than the shape [89]. The validation of all satellite-derived Rrs versus in situ measurements was then shown, proposing an aggregated representation for each of the three satellites. The local maximum of Rrs in the green region varies in the range of 0.020–0.030 sr⁻¹ for PRISMA images, and from 0.025 to 0.035 sr⁻¹ for DESIS images. The statistical results obtained in the case of PRISMA are comparable with those obtained in [34], i.e., R² = 0.87, and those obtained in [43], i.e., SA around 10° and MAPD around 30%. The in situ data synchronous with the DESIS images show greater variability than the other in situ measurements. The DESIS-derived Rrs show, on average, the best agreement in terms of spectral shape (statistically represented by SA), while the best agreement in terms of magnitude (RMSD, MAPD) is obtained for the EnMAP image. This could be attributed to the model implemented for atmospheric correction, which is designed specifically for water targets.

Once the Rrs products were validated and preliminary steps—such as the removal of noisy bands—were carried out, they were used as inputs into models for generating water quality products, which were then validated again by comparison with the in situ measurements, as performed in [90–92]. From the results of the statistical analysis, the finding that the highest level of agreement is obtained in the case of the TSM concentration maps generated by DESIS images may stem from the fact that in the radiometric statistical analysis of DESIS resulted in the lowest SA value and therefore the sensor with the highest spectral similarity compared to the in situ measurement. Generally, the maps obtained from the DESIS Rrs products seem to show greater variability in Chl-a and TSM concentrations; such an outcome may have arisen from the fact that, at the radiometric level, the standard deviation of both the satellite and in situ measurements was high, in the 700–800 nm range.

The synergetic use of the three hyperspectral sensors is a great advantage for carrying out a temporal analysis, useful, for instance, in understanding the dynamics of phytoplankton and TSM. Since the lake presents meso-eutrophic conditions with high seasonal variability, this variability can also be seen in the TSM concentrations, showing higher values near the tributary inflow, which is likely to transport suspended sediment loads from the catchment into the lake. The Chl-a values are, on average, increased in 2022, compared to previous years, at the same time as the lake level is decreasing; these two parameters are indeed negatively correlated, as stated in [93], a study conducted on Lake Trasimeno. The maximum values of PC and TSM are negatively correlated with lake levels (Pearson correlation, respectively: $r = -0.942$ and p value < 0.001 ; $r = -0.678$ and p value < 0.05), suggesting key roles of these parameters in lake ecology. In this work, it was possible to identify the trend of these optically active parameters and aquatic vegetation over the summer/late summer seasons of four years. The PC values range mainly from 0 to 25 mg/m³, which represents the suggested range for the use of the MDN, as reported by [37]. Once more, the statistical results achieved by comparing the products obtained from PRISMA images with the in situ measurements show comparable values with previous comparisons with Sentinel-2 [34], e.g., RMSD = 1.23 mg/m³ for the TSM concentration maps.

Both the coverage area and the WAVI vegetation index, a proxy for biomass density, calculated on emergent macrophytes, show a significant increase in 2022 compared to 2019, with several areas of the lake affected by this phenomenon. In a previous study [31] the aquatic vegetation of Lake Trasimeno was observed from an airborne AVIRIS image, and the results showed that the south-eastern zone was colonized by the three different submerged classes but not yet by the emergent macrophytes. In fact, this portion of the lake, in the

present study, exhibits a high level of variability (i.e., high standard deviation values) both for submerged and emergent macrophytes. To improve knowledge of the complex relations between primary producers (i.e., rooted macrophytes, phytoplankton and cyanobacteria), TSM and water clarity, hyperspectral maps can be a useful tool to support lake ecosystem analysis. It is well known that the loss of aquatic vegetation threatens water transparency due to the absence of mechanical and chemical processes mediated by macrophytes (e.g., the stabilization and prevention of sediment resuspension, refuges for zooplankton that feeds on microalgae, competition for nutrients and light and the production of allelopathic substances that counteract algal proliferation and dominance) [94,95]. In the limited dataset of this work, it indeed turns out that the average TSM values are generally lower on the dates with higher area values of submerged macrophytes. The widespread expansion of submerged macrophytes and the appearance of semi-emergent macrophytes above the water surface in 2022 should be actively monitored, as this is likely to be mainly due to the sharp drop in lake levels, accompanied by a reduction in both cumulative early June rainfall (−32% compared to 2021) and total annual rainfall (−20% compared to 2021). Indeed, the lake water level is significantly negatively correlated with the area of submerged and emergent macrophytes (Pearson correlation, respectively: $r = -0.659$ and p value < 0.05 ; $r = -0.959$ and p value < 0.001). In addition to water levels, the component of avifauna that feeds on submerged macrophytes turns out to be an important element in the variability of submerged macrophyte cover. Aquatic plants are a fundamental element of biodiversity, i.e., the number of herbivores in Lake Trasimeno [96]. In fact, in 2020, when the submerged macrophytes were more abundant than in the previous and in the following years, the number of herbivorous birds was much lower (about 30%); this number then became more stable as the submerged macrophytes stabilized. Although the present study provides promising insights into the mapping of aquatic ecosystems with hyperspectral images, it is important to acknowledge several limitations. Firstly, to increase the robustness of the analysis, it would be necessary to assess the uncertainty related to the atmospheric correction that can propagate into errors in the retrieved satellite products. Additionally, expanding the dataset would provide wider temporal coverage, crucial for this kind of analysis. Finally, in the fundamental step of satellite products validation, it would be essential to collect more spatially distributed in situ samples to increase the robustness of the statistics, and to consider the use of water quality data as derived from laboratory analyses of water samples, which, unfortunately, were not planned to be collected at the time of satellite overpasses. According to [23], efforts have still to be made toward the integration of remote sensing with traditional monitoring programs for coordinating water authorities' strategies with the remote sensing observation requirements.

5. Conclusions

This study demonstrates the feasibility of the use of standard L2 products provided by the spaceborne hyperspectral PRISMA, DESIS and EnMAP missions to detect spatio-temporal variations in water quality parameters and aquatic vegetation in optically deep and shallow inland waters characterized by moderately high Rrs values. The validation results showed that hyperspectral satellite images can be successfully used to capture a comprehensive picture of Lake Trasimeno's water quality that can be integrated with conventional ground-based monitoring programs. The results obtained confirm the advantage of hyperspectral data, characterized by numerous narrow bands in the VNIR domain, in order to be able to simultaneously quantify concentrations of phytoplankton pigments, such as Chl-a and PC; TSM; and the extent and type of submerged and emergent macrophytes, hence contributing to the satellite-based mapping of standard (e.g., Chl-a, TSM) and advanced (e.g., PC, shallow waters) aquatic ecosystem products. The method outlined in this paper confirms the robustness of sensor-independent approaches such as the bio-optical model BOMBER, while the similar spectral setting of the three missions allowed us to adapt the MDN, originally tested for PRISMA, to DESIS and EnMAP imagery data. Nonetheless, pre-processing techniques, necessary, for instance, to remove sun glint and decrease the

environmental noise of imagery data, might be necessary for applying similar approaches to other inland waters, at least for those with optical water types similar to the one analyzed in this study. These results highlight the significant degree of temporal and spatial changes in the primary producers and aquatic vegetation in Lake Trasimeno; it has been shown that the water level is a fundamental factor in determining the ecosystem conditions of Lake Trasimeno and, hence, in conditioning its biodiversity and the complex trophic and physical relations that govern the management of these areas. Further analyses would increase the robustness of this study, for instance, by testing different atmospheric correction models, increasing the dataset and collecting multiple radiometric measurements and water samples for more distributed and comprehensive validation of the satellite products. Such additional work will also boost the advantages of exploiting hyperspectral satellite data for monitoring dynamic processes and changes over time, laying the foundation for routine monitoring, in view of future operative hyperspectral missions (e.g., CHIME, SBG and PRISMA 2nd generation).

Author Contributions: Conceptualization, A.F., M.B. and C.G.; methodology, A.F., M.B., A.P. and C.G.; validation, A.F., M.B., S.M., R.P. and M.P.; formal analysis, A.F. and A.P.; investigation, A.F., M.B., A.P., M.P., K.A., S.M. and R.P.; data curation, A.F., M.B. and A.P.; writing—original draft preparation, A.F., M.B., A.P., M.P. and C.G.; writing—review and editing, A.F., M.B., A.P., M.P., K.A., R.P. and C.G.; supervision, K.A. and C.G. All authors have read and agreed to the published version of the manuscript.

Funding: This work was supported by funding from the agreement ASI-CNR, n. 20195HH0 “Attività scientifica di CAL/VAL della missione PRISMA, PRISCAV” and the project ASI-CNR, n. 2022-15-U.0 “PRISMA Products AND Applications for inland and coastal WATER, PANDA-WATER”. The authors acknowledge the support of NBFC to CNR, funded by the Italian Ministry of University and Research, PNRR, Missione 4 Componente 2, “Dalla ricerca all’impresa”, Investimento 1.4, Project CN00000033.

Data Availability Statement: The datasets generated and/or analyzed during the current study are available from the corresponding author on reasonable request.

Acknowledgments: We are very grateful to R. Bolpagni, E. Piaser, L. Panizza and N. Ghirardi for the useful discussion for the analysis developed in this study. We would like to thank the “Cooperativa dei Pescatori del Trasimeno” for their support in the field campaigns. We are very grateful to E. Lopinto and P. Sacco from ASI, to N. Pinnel and U. Heiden from DLR and to M. Soppa from AWI for the relevant discussions on the PRISMA, DESIS and EnMAP missions. We would like to thank the two anonymous reviewers for their help in improving the quality of the study.

Conflicts of Interest: The authors declare no conflicts of interest.

References

1. Adrian, R.; O’Reilly, C.M.; Zagarese, H.; Baines, S.B.; Hessen, D.O.; Keller, W.; Livingstone, D.M.; Sommaruga, R.; Straile, D.; Van Donk, E.; et al. Lakes as Sentinels of Climate Change. *Limnol. Oceanogr.* **2009**, *54*, 2283–2297. [[CrossRef](#)] [[PubMed](#)]
2. Rose, K.C.; Bierwagen, B.; Bridgman, S.D.; Carlisle, D.M.; Hawkins, C.P.; Poff, N.L.; Read, J.S.; Rohr, J.R.; Saros, J.E.; Williamson, C.E. Indicators of the Effects of Climate Change on Freshwater Ecosystems. *Clim. Chang.* **2023**, *176*, 23. [[CrossRef](#)]
3. Chapman, D.V.; Sullivan, T. The Role of Water Quality Monitoring in the Sustainable Use of Ambient Waters. *One Earth* **2022**, *5*, 132–137. [[CrossRef](#)]
4. Carvalho, L.; Mackay, E.B.; Cardoso, A.C.; Baattrup-Pedersen, A.; Birk, S.; Blackstock, K.L.; Borics, G.; Borja, A.; Feld, C.K.; Ferreira, M.T.; et al. Protecting and Restoring Europe’s Waters: An Analysis of the Future Development Needs of the Water Framework Directive. *Sci. Total Environ.* **2019**, *658*, 1228–1238. [[CrossRef](#)] [[PubMed](#)]
5. Alikas, K.; Kangro, K.; Randoja, R.; Philipson, P.; Asuküll, E.; Pisek, J.; Reinart, A. Satellite-Based Products for Monitoring Optically Complex Inland Waters in Support of EU Water Framework Directive. *Int. J. Remote Sens.* **2015**, *36*, 4446–4468. [[CrossRef](#)]
6. European Commission Water Framework Directive. Available online: https://environment.ec.europa.eu/topics/water/water-framework-directive_en (accessed on 5 March 2024).
7. Kratzer, S.; Harvey, E.T.; Canuti, E. International Intercomparison of In Situ Chlorophyll-a Measurements for Data Quality Assurance of the Swedish Monitoring Program. *Front. Remote Sens.* **2022**, *3*, 866712. [[CrossRef](#)]
8. Zhai, M.; Zhou, X.; Tao, Z.; Lv, T.; Zhang, H.; Li, R.; Huang, Y. Retrieve of Total Suspended Matter in Typical Lakes in China Based on Broad Bandwidth Satellite Data: Random Forest Model with Forel-Ule Index. *Front. Environ. Sci.* **2023**, *11*, 1132346. [[CrossRef](#)]

9. Wen, Z.; Wang, Q.; Ma, Y.; Jacinthe, P.A.; Liu, G.; Li, S.; Shang, Y.; Tao, H.; Fang, C.; Lyu, L.; et al. Remote Estimates of Suspended Particulate Matter in Global Lakes Using Machine Learning Models. *Int. Soil Water Conserv. Res.* **2024**, *12*, 200–216. [[CrossRef](#)]
10. Lyu, L.; Song, K.; Wen, Z.; Liu, G.; Fang, C.; Shang, Y.; Li, S.; Tao, H.; Wang, X.; Li, Y.; et al. Remote Estimation of Phycocyanin Concentration in Inland Waters Based on Optical Classification. *Sci. Total Environ.* **2023**, *899*, 166363. [[CrossRef](#)] [[PubMed](#)]
11. Cazzaniga, I.; Zibordi, G.; Mélin, F. Spectral Features of Ocean Colour Radiometric Products in the Presence of Cyanobacteria Blooms in the Baltic Sea. *Remote Sens. Environ.* **2023**, *287*, 113464. [[CrossRef](#)]
12. Roelfsema, C.; Dennison, B.; Phinn, S.; Dekker, A.; Brando, V. Remote Sensing of a Cyanobacterial Bloom (*Lyngbya majuscula*) in Moreton Bay, Australia. In Proceedings of the IGARSS 2001. Scanning the Present and Resolving the Future. Proceedings. IEEE 2001 International Geoscience and Remote Sensing Symposium (Cat. No.01CH37217), Sydney, Australia, 9–13 July 2001; pp. 613–615.
13. Jeppesen, E.; Peder Jensen, J.; Søndergaard, M.; Lauridsen, T.; Junge Pedersen, L.; Jensen, L. Top-down Control in Freshwater Lakes: The Role of Nutrient State, Submerged Macrophytes and Water Depth. In *Shallow Lakes '95*; Springer: Dordrecht, The Netherlands, 1997; pp. 151–164.
14. Piaser, E.; Berton, A.; Bolpagni, R.; Caccia, M.; Castellani, M.B.; Coppi, A.; Vecchia, A.D.; Gallivanone, F.; Sona, G.; Villa, P. Impact of Radiometric Variability on Ultra-High Resolution Hyperspectral Imagery Over Aquatic Vegetation: Preliminary Results. *IEEE J. Sel. Top. Appl. Earth Obs. Remote Sens.* **2023**, *16*, 5935–5950. [[CrossRef](#)]
15. Liang, S.; Gong, Z.; Wang, Y.; Zhao, J.; Zhao, W. Accurate Monitoring of Submerged Aquatic Vegetation in a Macrophytic Lake Using Time-Series Sentinel-2 Images. *Remote Sens.* **2022**, *14*, 640. [[CrossRef](#)]
16. Carr, J.; D'Odorico, P.; McGlathery, K.; Wiberg, P. Stability and Bistability of Seagrass Ecosystems in Shallow Coastal Lagoons: Role of Feedbacks with Sediment Resuspension and Light Attenuation. *J. Geophys. Res. Biogeosci.* **2010**, *115*, G3. [[CrossRef](#)]
17. Adjovu, G.E.; Stephen, H.; James, D.; Ahmad, S. Overview of the Application of Remote Sensing in Effective Monitoring of Water Quality Parameters. *Remote Sens.* **2023**, *15*, 1938. [[CrossRef](#)]
18. Cao, Q.; Yu, G.; Qiao, Z. Application and Recent Progress of Inland Water Monitoring Using Remote Sensing Techniques. *Environ. Monit. Assess.* **2023**, *195*, 125. [[CrossRef](#)] [[PubMed](#)]
19. Odermatt, D.; Gitelson, A.; Brando, V.E.; Schaepman, M. Review of Constituent Retrieval in Optically Deep and Complex Waters from Satellite Imagery. *Remote Sens. Environ.* **2012**, *118*, 116–126. [[CrossRef](#)]
20. Tyler, A.N.; Hunter, P.D.; Spyarakos, E.; Groom, S.; Constantinescu, A.M.; Kitchen, J. Developments in Earth Observation for the Assessment and Monitoring of Inland, Transitional, Coastal and Shelf-Sea Waters. *Sci. Total Environ.* **2016**, *572*, 1307–1321. [[CrossRef](#)] [[PubMed](#)]
21. Birk, S.; Ecke, F. The Potential of Remote Sensing in Ecological Status Assessment of Coloured Lakes Using Aquatic Plants. *Ecol. Indic.* **2014**, *46*, 398–406. [[CrossRef](#)]
22. Phinn, S.; Roelfsema, C.; Dekker, A.; Brando, V.; Anstee, J. Mapping Seagrass Species, Cover and Biomass in Shallow Waters: An Assessment of Satellite Multi-Spectral and Airborne Hyper-Spectral Imaging Systems in Moreton Bay (Australia). *Remote Sens. Environ.* **2008**, *112*, 3413–3425. [[CrossRef](#)]
23. Topp, S.N.; Pavelsky, T.M.; Jensen, D.; Simard, M.; Ross, M.R.V. Research Trends in the Use of Remote Sensing for Inland Water Quality Science: Moving Towards Multidisciplinary Applications. *Water* **2020**, *12*, 169. [[CrossRef](#)]
24. Samarinas, N.; Spiliotopoulos, M.; Tziolas, N.; Loukas, A. Synergistic Use of Earth Observation Driven Techniques to Support the Implementation of Water Framework Directive in Europe: A Review. *Remote Sens.* **2023**, *15*, 1983. [[CrossRef](#)]
25. Rast, M.; Painter, T.H. Earth Observation Imaging Spectroscopy for Terrestrial Systems: An Overview of Its History, Techniques, and Applications of Its Missions. *Surv. Geophys.* **2019**, *40*, 303–331. [[CrossRef](#)]
26. Dey, J.; Vijay, R. A Critical and Intensive Review on Assessment of Water Quality Parameters through Geospatial Techniques. *Environ. Sci. Pollut. Res.* **2021**, *28*, 41612–41626. [[CrossRef](#)] [[PubMed](#)]
27. Leiper, I.; Phinn, S.; Roelfsema, C.; Joyce, K.; Dekker, A. Mapping Coral Reef Benthos, Substrates, and Bathymetry, Using Compact Airborne Spectrographic Imager (CASI) Data. *Remote Sens.* **2014**, *6*, 6423–6445. [[CrossRef](#)]
28. Vahtmäe, E.; Paavel, B.; Kutser, T. How Much Benthic Information Can Be Retrieved with Hyperspectral Sensor from the Optically Complex Coastal Waters? *J. Appl. Remote Sens.* **2020**, *14*, 1. [[CrossRef](#)]
29. Turpie, K.R.; Klemas, V.V.; Byrd, K.; Kelly, M.; Jo, Y.-H. Prospective HypsIRI Global Observations of Tidal Wetlands. *Remote Sens. Environ.* **2015**, *167*, 206–217. [[CrossRef](#)]
30. Chander, S.; Pompapathi, V.; Gujrati, A.; Singh, R.P.; Chaplot, N.; Patel, U.D. GROWTH OF INVASIVE AQUATIC MACROPHYTES OVER TAPI RIVER. *Int. Arch. Photogramm. Remote Sens. Spat. Inf. Sci.* **2018**, *XLII-5*, 829–833. [[CrossRef](#)]
31. Giardino, C.; Bresciani, M.; Valentini, E.; Gasperini, L.; Bolpagni, R.; Brando, V.E. Airborne Hyperspectral Data to Assess Suspended Particulate Matter and Aquatic Vegetation in a Shallow and Turbid Lake. *Remote Sens. Environ.* **2015**, *157*, 48–57. [[CrossRef](#)]
32. Adam, E.; Mutanga, O.; Rugege, D. Multispectral and Hyperspectral Remote Sensing for Identification and Mapping of Wetland Vegetation: A Review. *Wetl. Ecol. Manag.* **2010**, *18*, 281–296. [[CrossRef](#)]
33. Bresciani, M.; Giardino, C.; Fabbretto, A.; Pellegrino, A.; Mangano, S.; Free, G.; Pinardi, M. Application of New Hyperspectral Sensors in the Remote Sensing of Aquatic Ecosystem Health: Exploiting PRISMA and DESIS for Four Italian Lakes. *Resources* **2022**, *11*, 8. [[CrossRef](#)]

34. Niroumand-Jadidi, M.; Bovolo, F.; Bruzzone, L. Water Quality Retrieval from PRISMA Hyperspectral Images: First Experience in a Turbid Lake and Comparison with Sentinel-2. *Remote Sens.* **2020**, *12*, 3984. [[CrossRef](#)]
35. Soppa, M.A.; Dinh, D.A.; Silva, B.; Steinmetz, F.; Alvarado, L.; Bracher, A. INTERCOMPARISON OF DESIS, SENTINEL-2 (MSI) AND SENTINEL-3 (OLCI) DATA FOR WATER COLOUR APPLICATIONS. *Int. Arch. Photogramm. Remote Sens. Spat. Inf. Sci.* **2022**, *XLVI-1/W1-2021*, 69–72. [[CrossRef](#)]
36. Katlane, R.; Doxaran, D.; ElKilani, B.; Trabelsi, C. Remote Sensing of Turbidity in Optically Shallow Waters Using Sentinel-2 MSI and PRISMA Satellite Data. *PFQ—J. Photogramm. Remote Sens. Geoinf. Sci.* **2023**, 1–17. [[CrossRef](#)]
37. O’Shea, R.E.; Pahlevan, N.; Smith, B.; Bresciani, M.; Egerton, T.; Giardino, C.; Li, L.; Moore, T.; Ruiz-Verdu, A.; Ruberg, S.; et al. Advancing Cyanobacteria Biomass Estimation from Hyperspectral Observations: Demonstrations with HICO and PRISMA Imagery. *Remote Sens. Environ.* **2021**, *266*, 112693. [[CrossRef](#)]
38. Taggio, N.; Aiello, A.; Ceriola, G.; Kremezi, M.; Kristollari, V.; Kolokoussis, P.; Karathanassi, V.; Barbone, E. A Combination of Machine Learning Algorithms for Marine Plastic Litter Detection Exploiting Hyperspectral PRISMA Data. *Remote Sens.* **2022**, *14*, 3606. [[CrossRef](#)]
39. Justice, C.; Belward, A.; Morisette, J.; Lewis, P.; Privette, J.; Baret, F. Developments in the “validation” of Satellite Sensor Products for the Study of the Land Surface. *Int. J. Remote Sens.* **2000**, *21*, 3383–3390. [[CrossRef](#)]
40. Concha, J.A.; Bracaglia, M.; Brando, V.E. Assessing the Influence of Different Validation Protocols on Ocean Colour Match-up Analyses. *Remote Sens. Environ.* **2021**, *259*, 112415. [[CrossRef](#)]
41. Sterckx, S.; Brown, I.; Käab, A.; Krol, M.; Morrow, R.; Veeffkind, P.; Boersma, K.F.; De Mazière, M.; Fox, N.; Thorne, P. Towards a European Cal/Val Service for Earth Observation. *Int. J. Remote Sens.* **2020**, *41*, 4496–4511. [[CrossRef](#)]
42. Giardino, C.; Bresciani, M.; Braga, F.; Fabbretto, A.; Ghirardi, N.; Pepe, M.; Gianinetto, M.; Colombo, R.; Cogliati, S.; Ghebrehiwot, S.; et al. First Evaluation of PRISMA Level 1 Data for Water Applications. *Sensors* **2020**, *20*, 4553. [[CrossRef](#)] [[PubMed](#)]
43. Braga, F.; Fabbretto, A.; Vanhellemont, Q.; Bresciani, M.; Giardino, C.; Scarpa, G.M.; Manfè, G.; Concha, J.A.; Brando, V.E. Assessment of PRISMA Water Reflectance Using Autonomous Hyperspectral Radiometry. *ISPRS J. Photogramm. Remote Sens.* **2022**, *192*, 99–114. [[CrossRef](#)]
44. Pellegrino, A.; Fabbretto, A.; Bresciani, M.; de Lima, T.M.A.; Braga, F.; Pahlevan, N.; Brando, V.E.; Kratzer, S.; Gianinetto, M.; Giardino, C. Assessing the Accuracy of PRISMA Standard Reflectance Products in Globally Distributed Aquatic Sites. *Remote Sens.* **2023**, *15*, 2163. [[CrossRef](#)]
45. Mélin, F. Validation of Ocean Color Remote Sensing Reflectance Data: Analysis of Results at European Coastal Sites. *Remote Sens. Environ.* **2022**, *280*, 113153. [[CrossRef](#)]
46. Zibordi, G.; Ruddick, K.; Ansko, I.; Moore, G.; Kratzer, S.; Icely, J.; Reinart, A. In Situ Determination of the Remote Sensing Reflectance: An Inter-Comparison. *Ocean Sci.* **2012**, *8*, 567–586. [[CrossRef](#)]
47. Bresciani, M.; Pinardi, M.; Free, G.; Luciani, G.; Ghebrehiwot, S.; Laanen, M.; Peters, S.; Della Bella, V.; Padula, R.; Giardino, C. The Use of Multisource Optical Sensors to Study Phytoplankton Spatio-Temporal Variation in a Shallow Turbid Lake. *Water* **2020**, *12*, 284. [[CrossRef](#)]
48. Landucci, F.; Gigante, D.; Venanzoni, R. An Application of the Cocktail Method for the Classification of the Hydrophytic Vegetation at Lake Trasimeno (Central Italy). *Fitosociologia* **2011**, *48*, 3–22.
49. Bolpagni, R. Macrophyte Richness and Aquatic Vegetation Complexity of the Lake Idro (Northern Italy). *Ann. Bot.* **2013**, 35–43.
50. Bresciani, M.; Bolpagni, R.; Braga, F.; Oggioni, A.; Giardino, C. Retrospective Assessment of Macrophytic Communities in Southern Lake Garda (Italy) from in Situ and MIVIS (Multispectral Infrared and Visible Imaging Spectrometer) Data. *J. Limnol.* **2012**, *71*, 180–190. [[CrossRef](#)]
51. Melelli, A.; Fatichenti, F. Bacini idrografici e sfruttamento delle acque in Umbria. Tra passato e presente. Percorsi di ricerca, problemi, proposte. In *L’acqua in Umbria. Disponibilità, Consumo e Salute. Le Rappresentazioni e gli Atteggiamenti dei Cittadini*; ARPA Umbria: Terni, Italy, 2013; pp. 109–132.
52. Álvarez, X.; Valero, E.; Santos, R.M.B.; Varandas, S.G.P.; Sanches Fernandes, L.F.; Pacheco, F.A.L. Anthropogenic Nutrients and Eutrophication in Multiple Land Use Watersheds: Best Management Practices and Policies for the Protection of Water Resources. *Land. Use Policy* **2017**, *69*, 1–11. [[CrossRef](#)]
53. Regione Umbria Servizio Idrografico. Available online: <https://annali.regione.umbria.it/#> (accessed on 13 March 2024).
54. Peters, S.; Laanen, M.; Groetsch, P.; Ghezehegn, S.; Poser, K.; Hommersom, A.; De Reus, E.; Spaias, L. WISPstation: A New Autonomous above Water Radiometer System. In Proceedings of the Ocean Optics XXIV Conference, Dubrovnik, Croatia, 7 October 2018; pp. 7–12.
55. Riddick, C.; Tyler, A.; Hommersom, A.; Alikas, K.; Kangro, K.; Ligi, M.; Bresciani, M.; Antilla, S.; Vaiciute, D.; Bucas, M.; et al. EOMORES D5.3: Final Validation Report. 2019. Available online: <https://zenodo.org/records/4057057> (accessed on 9 May 2024).
56. Gons, H.J.; Rijkeboer, M.; Ruddick, K.G. Effect of a Waveband Shift on Chlorophyll Retrieval from MERIS Imagery of Inland and Coastal Waters. *J. Plankton Res.* **2004**, *27*, 125–127. [[CrossRef](#)]
57. Rijkeboer, M. *Algoritmen Voor Het Bepalen van de Concentratie Chlorofyl-a En Zwevend Stof Met de Optische Teledetectie Methode in Verschillende Optische Watertypen*; IVM Report; No. O-00/08; Dept. of Spatial Analysis and Decision Support: Amsterdam, The Netherlands, 2000.
58. Simis, S.G.H. Blue-Green Catastrophe: Remote Sensing of Mass Viral Lysis of Cyanobacteria. Ph.D. Thesis, Vrije Universiteit Amsterdam, Amsterdam, The Netherlands, 2006.

59. Giardino, C.; Bresciani, M.; Fava, F.; Matta, E.; Brando, V.; Colombo, R. Mapping Submerged Habitats and Mangroves of Lampi Island Marine National Park (Myanmar) from in Situ and Satellite Observations. *Remote Sens.* **2015**, *8*, 2. [CrossRef]
60. Regione Umbria Osservatorio Faunistico Regionale. Available online: <https://www.regione.umbria.it/turismo-attivita-sportive/osservatorio-faunistico> (accessed on 4 March 2024).
61. Cogliati, S.; Sarti, F.; Chiarantini, L.; Cosi, M.; Lorusso, R.; Lopinto, E.; Miglietta, F.; Genesio, L.; Guanter, L.; Damm, A.; et al. The PRISMA Imaging Spectroscopy Mission: Overview and First Performance Analysis. *Remote Sens. Environ.* **2021**, *262*, 112499. [CrossRef]
62. Kremezi, M.; Kristollari, V.; Karathanassi, V.; Topouzelis, K.; Kolokoussis, P.; Taggio, N.; Aiello, A.; Ceriola, G.; Barbone, E.; Corradi, P. Pansharpening PRISMA Data for Marine Plastic Litter Detection Using Plastic Indexes. *IEEE Access* **2021**, *9*, 61955–61971. [CrossRef]
63. Candela, L.; Formaro, R.; Guarini, R.; Loizzo, R.; Longo, F.; Varacalli, G. The PRISMA Mission. In Proceedings of the 2016 IEEE International Geoscience and Remote Sensing Symposium (IGARSS), Beijing, China, 10–15 July 2016; pp. 253–256.
64. Alonso, K.; Bachmann, M.; Burch, K.; Carmona, E.; Cerra, D.; de los Reyes, R.; Dietrich, D.; Heiden, U.; Hölderlin, A.; Ickes, J.; et al. Data Products, Quality and Validation of the DLR Earth Sensing Imaging Spectrometer (DESI). *Sensors* **2019**, *19*, 4471. [CrossRef] [PubMed]
65. Krutz, D.; Müller, R.; Knodt, U.; Günther, B.; Walter, I.; Sebastian, I.; Säuberlich, T.; Reulke, R.; Carmona, E.; Eckardt, A.; et al. The Instrument Design of the DLR Earth Sensing Imaging Spectrometer (DESI). *Sensors* **2019**, *19*, 1622. [CrossRef] [PubMed]
66. de los Reyes, R.; Langheinrich, M.; Schwind, P.; Richter, R.; Pflug, B.; Bachmann, M.; Müller, R.; Carmona, E.; Zekoll, V.; Reinartz, P. PACO: Python-Based Atmospheric Correction. *Sensors* **2020**, *20*, 1428. [CrossRef] [PubMed]
67. Habermeyer, M.; Pinnel, N.; Storch, T.; Honold, H.P.; Tucker, P.; Guanter, L.; Segl, K.; Fischer, S. The EnMAP Mission: From Observation Request to Data Delivery. In Proceedings of the IGARSS 2019—2019 IEEE International Geoscience and Remote Sensing Symposium, Yokohama, Japan, 28 July–2 August 2019; pp. 4507–4510.
68. Guanter, L.; Kaufmann, H.; Segl, K.; Foerster, S.; Rogass, C.; Chabrillat, S.; Kuester, T.; Hollstein, A.; Rossner, G.; Chlebek, C.; et al. The EnMAP Spaceborne Imaging Spectroscopy Mission for Earth Observation. *Remote Sens.* **2015**, *7*, 8830–8857. [CrossRef]
69. Kiselev, V.; Bulgarelli, B.; Heege, T. Sensor Independent Adjacency Correction Algorithm for Coastal and Inland Water Systems. *Remote Sens. Environ.* **2015**, *157*, 85–95. [CrossRef]
70. Storch, T.; Honold, H.-P.; Chabrillat, S.; Habermeyer, M.; Tucker, P.; Brell, M.; Ohndorf, A.; Wirth, K.; Betz, M.; Kuchler, M.; et al. The EnMAP Imaging Spectroscopy Mission towards Operations. *Remote Sens. Environ.* **2023**, *294*, 113632. [CrossRef]
71. ASI—Italian Space Agency PRISMA Algorithm Theoretical Basis Document (ATBD). Available online: <http://prisma.asi.it/missionselect/docs.php> (accessed on 18 January 2024).
72. DLR—German Space Agency DESIS Instrument. Available online: https://www.dlr.de/eoc/desktopdefault.aspx/tabid-13622/23667_read-54280/ (accessed on 4 March 2024).
73. DLR—German Space Agency EnMAP Specification. Available online: <https://www.enmap.org/mission/> (accessed on 4 March 2024).
74. Hedley, J.D.; Harborne, A.R.; Mumby, P.J. Technical Note: Simple and Robust Removal of Sun Glint for Mapping Shallow-water Benthos. *Int. J. Remote Sens.* **2005**, *26*, 2107–2112. [CrossRef]
75. Campbell, G.; Stuart, R. Phinn An Assessment of the Accuracy and Precision of Water Quality Parameters Retrieved with the Matrix Inversion Method. *Limnol. Ocean. Methods* **2010**, *8*, 16–29.
76. Soomets, T.; Uudeberg, K.; Jakovels, D.; Brauns, A.; Zagars, M.; Kutser, T. Validation and Comparison of Water Quality Products in Baltic Lakes Using Sentinel-2 MSI and Sentinel-3 OLCI Data. *Sensors* **2020**, *20*, 742. [CrossRef] [PubMed]
77. Vanhellefont, Q.; Ruddick, K. Acolite for Sentinel-2: Aquatic Applications of MSI Imagery. In Proceedings of the 2016 ESA Living Planet Symposium, Prague, Czech Republic, 9 May 2016.
78. Sagayam, K.M.; Bruntha, P.M.; Sridevi, M.; Renith Sam, M.; Kose, U.; Deperlioglu, O. A Cognitive Perception on Content-Based Image Retrieval Using an Advanced Soft Computing Paradigm. In *Advanced Machine Vision Paradigms for Medical Image Analysis*; Elsevier: Amsterdam, The Netherlands, 2021; pp. 189–211.
79. Villa, P.; Pinardi, M.; Tóth, V.R.; Hunter, P.D.; Bolpagni, R.; Bresciani, M. Remote Sensing of Macrophyte Morphological Traits: Implications for the Management of Shallow Lakes. *J. Limnol.* **2017**, *76*, 109–126. [CrossRef]
80. Lee, Z.; Carder, K.L.; Mobley, C.D.; Steward, R.G.; Patch, J.S. Hyperspectral Remote Sensing for Shallow Waters I A Semianalytical Model. *Appl. Opt.* **1998**, *37*, 6329. [CrossRef] [PubMed]
81. Lee, Z.; Carder, K.L.; Mobley, C.D.; Steward, R.G.; Patch, J.S. Hyperspectral Remote Sensing for Shallow Waters: 2 Deriving Bottom Depths and Water Properties by Optimization. *Appl. Opt.* **1999**, *38*, 3831. [CrossRef] [PubMed]
82. Github (MDN). Available online: <https://github.com/STREAM-RS/STREAM-RS> (accessed on 4 March 2024).
83. Kutser, T.; Metsamaa, L.; Strömbeck, N.; Vahtmäe, E. Monitoring Cyanobacterial Blooms by Satellite Remote Sensing. *Estuar. Coast. Shelf Sci.* **2006**, *67*, 303–312. [CrossRef]
84. Zibordi, G.; Mélin, F.; Berthon, J.-F.; Holben, B.; Slutsker, I.; Giles, D.; D’Alimonte, D.; Vandemark, D.; Feng, H.; Schuster, G.; et al. AERONET-OC: A Network for the Validation of Ocean Color Primary Products. *J. Atmos. Ocean. Technol.* **2009**, *26*, 1634–1651. [CrossRef]
85. Bailey, S.W.; Franz, B.A.; Werdell, P.J. Estimation of Near-Infrared Water-Leaving Reflectance for Satellite Ocean Color Data Processing. *Opt. Express* **2010**, *18*, 7521. [CrossRef] [PubMed]

86. McCarthy, S.; Gould, R.; Richman, J.; Kearney, C.; Lawson, A. Impact of Aerosol Model Selection on Water-Leaving Radiance Retrievals from Satellite Ocean Color Imagery. *Remote Sens.* **2012**, *4*, 3638–3665. [[CrossRef](#)]
87. Schaepman, M.E.; Jehle, M.; Hueni, A.; D'Odorico, P.; Damm, A.; Weyermann, J.; Schneider, F.D.; Laurent, V.; Popp, C.; Seidel, F.C.; et al. Advanced Radiometry Measurements and Earth Science Applications with the Airborne Prism Experiment (APEX). *Remote Sens. Environ.* **2015**, *158*, 207–219. [[CrossRef](#)]
88. González Vilas, L.; Brando, V.E.; Concha, J.A.; Goyens, C.; Dogliotti, A.I.; Doxaran, D.; Dille, A.; Van der Zande, D. Validation of Satellite Water Products Based on HYPERNETS in Situ Data Using a Match-up Database (MDB) File Structure. *Front. Remote Sens.* **2024**, *5*, 1330317. [[CrossRef](#)]
89. Zhang, H.; Wang, M. Evaluation of Sun Glint Models Using MODIS Measurements. *J. Quant. Spectrosc. Radiat. Transf.* **2010**, *111*, 492–506. [[CrossRef](#)]
90. Di Francesco, S.; Venturi, S.; Casadei, S. An Integrated Water Resource Management Approach for Lake Trasimeno, Italy. *Hydrol. Sci. J.* **2023**, *68*, 630–644. [[CrossRef](#)]
91. Chebud, Y.; Naja, G.M.; Rivero, R.G.; Melesse, A.M. Water Quality Monitoring Using Remote Sensing and an Artificial Neural Network. *Water Air Soil Pollut.* **2012**, *223*, 4875–4887. [[CrossRef](#)]
92. Su, Y.-F.; Liou, J.-J.; Hou, J.-C.; Hung, W.-C.; Hsu, S.-M.; Lien, Y.-T.; Su, M.-D.; Cheng, K.-S.; Wang, Y.-F. A Multivariate Model for Coastal Water Quality Mapping Using Satellite Remote Sensing Images. *Sensors* **2008**, *8*, 6321–6339. [[CrossRef](#)] [[PubMed](#)]
93. Giardino, C.; Bresciani, M.; Villa, P.; Martinelli, A. Application of Remote Sensing in Water Resource Management: The Case Study of Lake Trasimeno, Italy. *Water Resour. Manag.* **2010**, *24*, 3885–3899. [[CrossRef](#)]
94. Marzocchi, U.; Benelli, S.; Larsen, M.; Bartoli, M.; Glud, R.N. Spatial Heterogeneity and Short-term Oxygen Dynamics in the Rhizosphere of *Vallisneria Spiralis*: Implications for Nutrient Cycling. *Freshw. Biol.* **2019**, *64*, 532–543. [[CrossRef](#)]
95. Licci, S.; Nepf, H.; Delolme, C.; Marmonier, P.; Bouma, T.J.; Puijalon, S. The Role of Patch Size in Ecosystem Engineering Capacity: A Case Study of Aquatic Vegetation. *Aquat. Sci.* **2019**, *81*, 41. [[CrossRef](#)]
96. Janssen, A.B.G.; Hilt, S.; Kosten, S.; de Klein, J.J.M.; Paerl, H.W.; Van de Waal, D.B. Shifting States, Shifting Services: Linking Regime Shifts to Changes in Ecosystem Services of Shallow Lakes. *Freshw. Biol.* **2021**, *66*, 1–12. [[CrossRef](#)]

Disclaimer/Publisher's Note: The statements, opinions and data contained in all publications are solely those of the individual author(s) and contributor(s) and not of MDPI and/or the editor(s). MDPI and/or the editor(s) disclaim responsibility for any injury to people or property resulting from any ideas, methods, instructions or products referred to in the content.